

Probing the Interfacial Properties of ACIGS Solar Cells with Targeted Proton Irradiation

Sergio A. Chacon, Megh N. Khanal, Brandon K. Durant, Hadi Afshari, Todd A. Byers, Mritunjaya Parashar, Bibhudutta Rout, Vincent R. Whiteside, Dmitry Poplavskyy, and Ian R. Sellers\*

ACIGS solar cells are exposed to targeted radiation to probe the front and back interfaces of the absorber to assess the impact of space environments on these systems. These data suggest ACIGS cells are more radiation-hard than early CIGS devices likely due to the lower defect densities and more ideal interfaces in the ACIGS system. A combination of J-V and external quantum efficiency measurements indicates some improvement in the performance of the device due to the effects of local heating in the dominant ionizing electronic energy loss regime of proton irradiation that anneal the upper CdS/ACIGS interface. However, nonionizing energy losses at the base of the solar cell also appear to inhibit minority carrier collection from the back of the cell at the ACIGS/Mo interface, which is discussed in terms of defect-mediated changes in the doping profile, the Ga/Ga+In ratio, and impurity composition after proton irradiation.

1. Introduction

I. R. Sellers

Cu(In,Ga)Se<sub>2</sub> (CIGS) solar cells have shown themselves to be both commercially reliable and a rich environment for continued research to further improve the performance of these systems. Currently, CIGS solar cells have surpassed 20% power conversion efficiency (PCE)<sup>[1]</sup> and CIGS have been used in tandem solar cells with some success. [2] In addition to their terrestrial successes, previous research has shown that CIGS devices have

2. Methodology

S. A. Chacon, M. N. Khanal, B. K. Durant, H. Afshari, V. R. Whiteside,

D. Poplavskyy MiaSolé Hi-Tech. Corp. Santa Clara, CA 95051, USA I. R. Sellers

Department of Electrical Engineering University at Buffalo SUNY Buffalo, NY 14260, USA

Department of Physics & Astronomy

University of Oklahoma Norman, OK 73019, USA

Department of Physics

University of North Texas

Denton, TX 76203, USA

E-mail: isellers@buffalo.edu

T. A. Byers, M. Parashar, B. Rout

The ORCID identification number(s) for the author(s) of this article can be found under https://doi.org/10.1002/solr.202300756.

DOI: 10.1002/solr.202300756

high radiation tolerance and perform well low-intensity low-temperature conditions.<sup>[3]</sup> The incorporation of silver to create ACIGS<sup>[4]</sup> brings several advantages in terms of both manufacturing and operation. Silver has been shown to lower the growth temperatures, increase grain size, lower structural disorder, and therefore consequently improve minority carrier collection length. [5-8] However, the role of bulk and interface defects, which encompass the absorber, and the metastable nature of the (A)CIGS absorber is still not well understood, particularly in the space environment.

This investigation seeks to build on the improvements and questions mentioned above as well as, the recent radiation study

on CIGS solar cells by Afshari et al. [9] These CIGS devices were irradiated with varying fluences of energetic protons to investigate the radiation hardness of this system. In this study, the relationship between the energy of protons and their implantation depths was used to assess the effects of radiation on specific interfaces and the nature of the resulting degradation to further evaluate the potential of the CIGS family for space power applications.

Here, two flexible ACIGS solar cells were assessed using materials supplied by MiaSolé Hi-Tech Corp. Devices cut from these flexible steel-based materials (that serve as the bottom contact of these structures) were fabricated into 64 mm<sup>2</sup> devices using standard photolithography processes, and thermal evaporation for the top aluminum contacts. The photovoltaic properties of the solar cells were assessed before and after irradiation using both broadband AM0 illumination (*J*–*V*) and external quantum efficiency (EQE) measurements. J-V data under AM0 conditions were collected using a Newport class ABA-solar simulator and a Keithley source measurement unit. EQE was taken using a quartz-tungsten halogen lamp and a calibrated silicon reference cell. AM0 J-V and EQEs were measured at temperatures ranging from 77 to 300 K using a liquid nitrogen-cooled Linkam cryostat.

After initial characterization, the two solar cells were sent to the University of North Texas Ion Beam Laboratory, where they underwent proton irradiation of 10<sup>11</sup> H<sup>+</sup>/cm<sup>2</sup> fluence.<sup>[10]</sup> www.advancedsciencenews.com



Protons were implanted with energies of 80 and 350 keV to target the front and back interfaces of the ACIGS absorber, respectively. The lower energy (80 keV) proton beams were extracted from a TiH solid cathode of a Source of Negative Ions by Cesium Sputtering (SNICS-II) associated with a 3 MV tandem Pelletron accelerator (NEC-9SDH-2). The higher energy (350 keV) proton beams were produced using a single-ended pelletron accelerator (NEC-9SDH) with an RF ion source. Momentum-analyzed proton beams were electrostatically raster scanned across the sample enabling uniform irradiation.

For the 80 keV proton beam, the irradiation was performed at an area of 3 cm² of the target through a circular aperture of 2 cm diameter, placed in front of the samples. For the 350 keV proton beam, the irradiation was performed at an area of 4 cm² by placing a square aperture (2 cm side). A beam flux of  $6.25 \times 10^9$  protons cm $^{-2}$ -sec was maintained during both the irradiation. To ensure uniform beam scanning, beam currents were monitored with four Faraday cups (3 mm² diameter) placed symmetrically around the circular aperture. Each irradiation lasted more than 15 s with multiple scanning passes to avoid any inhomogeneity within the beam spot.

After irradiation the samples were immediately shipped overnight and measured within 24 h at University of Oklahoma. The samples were package in vacuum-sealed air and light-tight containers for transit to prevent any external perturbations that may affect device performance outside of the radiation exposure.

Theoretical analysis of the proton implantations was performed using the Stopping and Range of Ions in Matter Simulator (SRIM) prior to the experiment. This software employs Monte Carlo simulations and calculates an implantation concentration and damage profile throughout the ion range in the device. The SRIM simulations were performed in the "Full damage cascades" mode for more than 200 000 ions. The target layers were taken as Layer-1: ZnO:Al 300 nm (density 4.21 g cm $^{-3}$ ), Layer-2: ZnO 100 nm (density 5.61 g cm $^{-3}$ ), Layer-3: CdS 40 nm (density 4.82 g cm $^{-3}$ ), Layer-4: ACIGS (Ag<sub>0.2</sub>Cu<sub>0.8</sub>In<sub>0.7</sub>Ga<sub>0.3</sub>)Se<sub>2</sub> 2000 nm (density 6. 433 g cm $^{-3}$ ), Layer-5: Mo 400 nm (density 10.20 g cm $^{-3}$ ), and Layer-6: stainless steel (substrate), density 8.05 g cm $^{-3}$ . To estimate the total damages (vacancies and displaced atoms), displacement energy for Al, Zn, Cd, S, Ag, Cu, In, Ga, Se, Mo was taken as 25 eV, and for O, it was 28 eV.

The SRIM simulations were then compared to EQE and J–V measurements that were measured before and after proton exposure to assess the effects of radiation on these systems.

#### 3. Results and Discussion

These devices under assessment were commercial-grade ACIGS materials supplied by MiaSolé Hi-Tech. Corp. with the following structure: ZnO:Al/i-ZnO/CdS/ACIGS/Mo/steel. The trajectories and stopping range of protons throughout the sample as calculated by SRIM are shown in **Figure 1**a for the sample exposed to 80 keV and in Figure 1b for the sample exposed to 350 keV. Both samples were irradiated through the front ZnO:Al surface to enable the use of low-energy protons that enable assessment of the upper emitter and high-energy protons to probe the base

region. The steel substrate prevented analysis (irradiation) in the reverse direction. In Figure 1, the protons enter from the left and are projected to the right. In this study, therefore, the front interface of both samples is exposed to irradiation.

Protons traveling through a device lose energy through two mechanisms: ionizing energy loss (IEL) and nonionizing energy loss (NIEL). IEL is the result of protons ionizing atoms and is responsible for localized heating. [12-14] Such localized heating can play a crucial role in annealing interfaces and therefore has the potential to provide a healing mechanism for damaged or nonideal interfaces. NIEL occurs when protons stop in the materials interacting through direct elastic collisions with nuclei of atoms and is a source of significant vacancy generation. [12-14] Such vacancies result in the creation of a number of defects including both displaced atoms (vacancies) and interstitials, as well as several multidefect complexes in CIGS<sup>[15,16]</sup> and ACIGS. [8] Moreover, the exact nature of these complexes can change due to external perturbations which affect the overall doping profile<sup>[9,15]</sup> and may increase or—via passivation—decrease the density of nonradiative centers in the device.

Figure 1c,d shows the IEL (black squares) and NIEL (red stars) throughout the cell for the 80 and 350 keV proton irradiated samples, respectively. In Figure 1, the contribution of IEL and NIEL determined by SRIM presented as a function of depth through the ACIGS solar cell structure evaluated. For the sample exposed to the 80 keV protons, only the first four layers of the structure are shown, since the projection of these lower energy protons only interacts with that region of the device (see Figure 1a). Respectively, the full structure of the device is shown in Figure 1d since 350 keV protons transverse the structure as is illustrated in Figure 1b. In Figure 1c,d, it is evident that the IEL is several orders of magnitude larger in both cases than the NIEL. The upper (front) emitter region (blue region of Figure 1c) of the solar cell exposed to 80 keV protons receives  $\approx$ 17.5 eV Å<sup>-1</sup> ions<sup>-1</sup> of IEL. In comparison, the input level of IEL for the front region of the solar cell exposed to 350 keV protons (blue region of Figure 1d) receives  $\approx 12.5 \text{ eV Å}^{-1} \text{ ions}^{-1}$ . However, by the time the radiation reaches the CdS/ACIGS interface, the IEL is approximately the same for both devices. Notably, the lower energy protons IEL decreases, while the high-energy protons IEL increases.

Close inspection of the SRIM simulations (Figure 1a,b) shows the 80 keV sample has a higher density of protons at the region surrounding the CdS than the device irradiated at 350 keV. There is a direct correlation between the density of protons and the quantity of IEL within a region. Examining beyond the CdS/ACIGS interface in Figure 1c for the simulations under 80 keV irradiation, there is a steep decline of IEL, while when exposing the sample to 350 keV (See Figure 1d) results in an increase in the contribution of IEL in the ACIGS region, which maximize is predicted to peak at the back of the ACIGS absorber prior to the Mo layer.

Here, the proton irradiation was designed such that NIEL processes were concentrated around the interfaces of interest. This is shown in Figure 1c,d where the NIEL losses are predicted to peak in the region of the front and back interfaces upon exposure to 80 keV and 350 keV, respectively. Importantly, the magnitudes of NIEL are also similar at the interfaces of both samples exposed ( $\approx 30 \, \mathrm{meV \, \mathring{A} \, ion}^{-1}$ ). This allows the physical effects under

2367198x, 0, Downloaded from https://onlinelibrary.wiley.com/doi/10.1002/solr.202300756 by National Yang Ming Chiao Tung Unive, Wiley Online Library on [18/12/2023]. See the Terms and Conditions (https://onlinelibrary.wiley.com/terms/

-and-conditions) on Wiley Online Library for rules of use; OA articles are governed by the applicable Creative Commons License

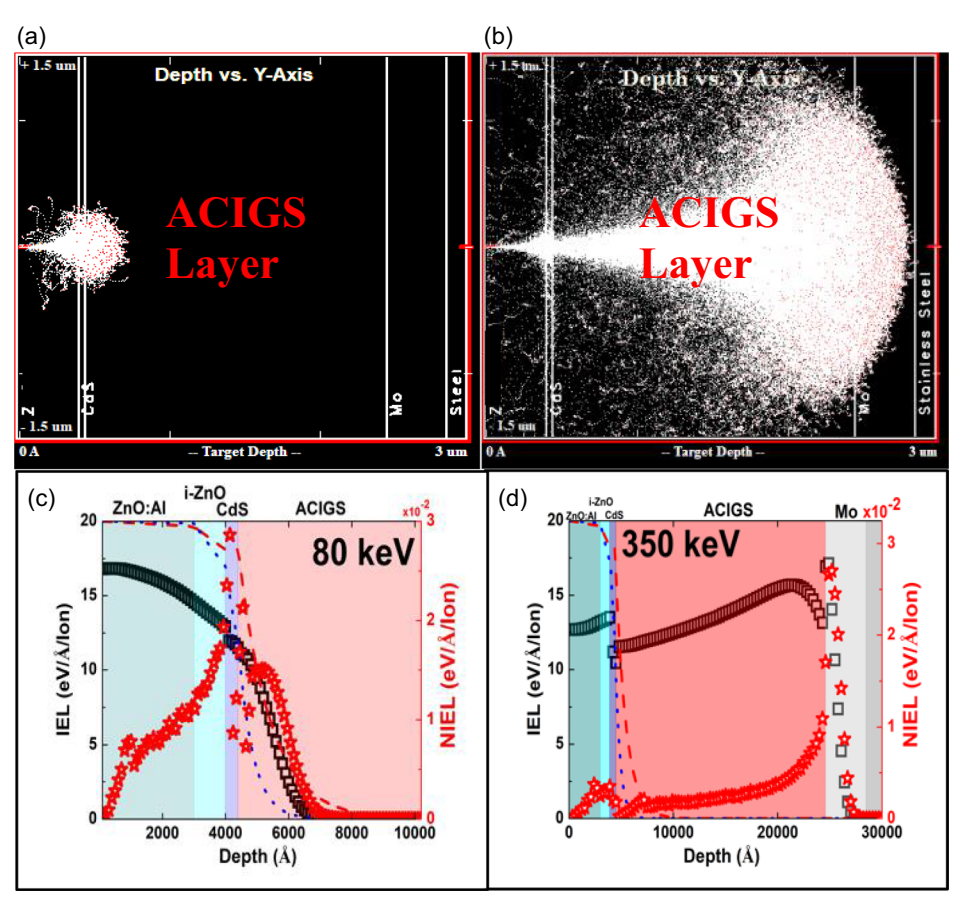


Figure 1. a) Proton stopping ranges for the sample exposed to 80 keV protons shown on top of the cell structure. b) Proton stopping ranges for the sample exposed to the 350 keV protons on top of the cell structure. c) IEL (black squares) and NIEL (red stars) as functions of depth for the device exposed to the 80 keV protons. These losses are shown on top of first four layers of the device structure, ZnO:Al/i-ZnO/CdS/ACIGS. d) IEL (black squares) and NIEL (red stars) as functions of depth for the device exposed to the 350 keV protons. These losses are shown on top of the entire device structure. ZnO:Al/i-ZnO/CdS/ACIGS/Mo/steel. The absorption of 442 nm and 633 nm lasers is plotted as dotted blue line and dashed red line respectively in (c) and (d).

different loss processes to be compared. While the 350 keV sample shows a NIEL peak at the CdS interface, this is less than  $5 \text{ meV Å}^{-1} \text{ ion}^{-1}$ . In comparison, the 80 keV sample has NIEL greater than 5 meV Å<sup>-1</sup> ion<sup>-1</sup> through the majority of the region before the CdS/ACIGS interface.

In addition to providing details with respect to NIEL, IEL, and stopping ranges or the projection of protons through the structure, SRIM also enables a qualitative estimation of the vacancies (or defects) generated by proton exposure. In addition to assessing the nature of the proton interaction in the structure, SRIM is also used to extract the nature of the vacancies in the solar cell, as shown in Figure 2. As in Figure 1c, in Figure 2a only the first four layers of the device structure are shown since all vacancies are created at the top of the device for the 80 keV exposure.

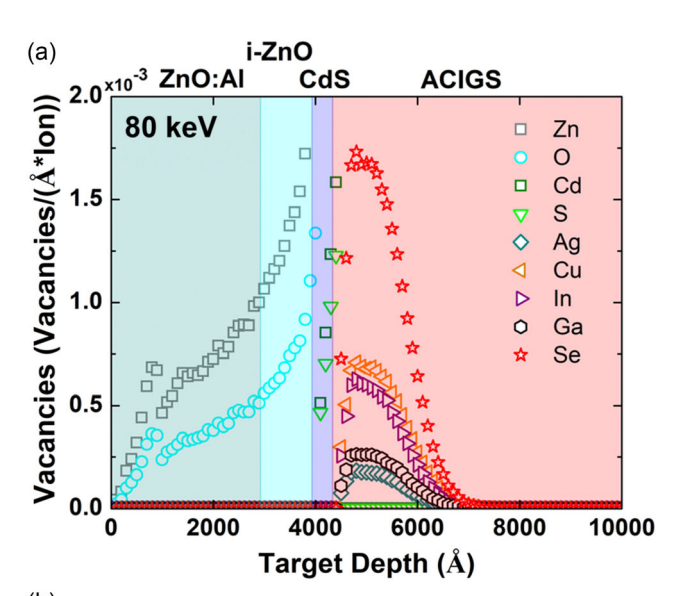
Under 80 keV exposure, at the upper emitter region of the device (ZnO/CdS region) shows a greater number of vacancies, which are predominantly created at the CdS/ACIGS interface due to the dominance of NIEL. This is significantly lower when the device is exposed to the 350 keV protons (Figure 2) since the higher energy protons travel further into the structure. Again, while SRIM indicates the density of displaced atoms (vacancies), the low formation energy of defects in CIGS-based structures<sup>[16]</sup> will undoubtedly lead to creation of several other related defect complexes affecting absorber, transport, and interface regions, as well as the doping profile of the device. While this is considered further later, the vacancy concentration discussed provides a good first-order approximation to the decomposition and defect generation in these systems.

The elemental analysis in Figure 2 follows to first order of the composition. For the 80 keV irradiation defects are generated in the ACIGS absorber at the CdS/ACIGS interface, within 100 nm of the absorber. The vacancies Se, Cu, and In, and to a lesser extent, Ga and Cd, are due to the prevalence of these elements in the ACIGS. Upon 350 keV exposure, similar effects are observed at the rear ACIGS/Mo interface. It is known that H+ interstitials can be electrically active defects. [17] Yet, unraveling how these defects manifest themselves as vacancies and interstitials is complex, particularly in ACIGS, which has a low defect formation energy, and suffers from metastabilities that affect the nature of the intrinsic doping and profile in these systems. These complexities arise from the fact that H<sup>+</sup> is mobile at room www.advancedsciencenews.com

www.solar-rrl.com

2367198x, 0, Downloaded from https://onlinelibrary.wiley.com/doi/10.1002/solr.202300756 by National Yang Ming Chiao Tung Unive, Wiley Online Library on [18/12/2023]. See the Terms and Conditions (https://onlinelibrary.wiley.

nditions) on Wiley Online Library for rules of use; OA articles are governed by the applicable Creative Commons License



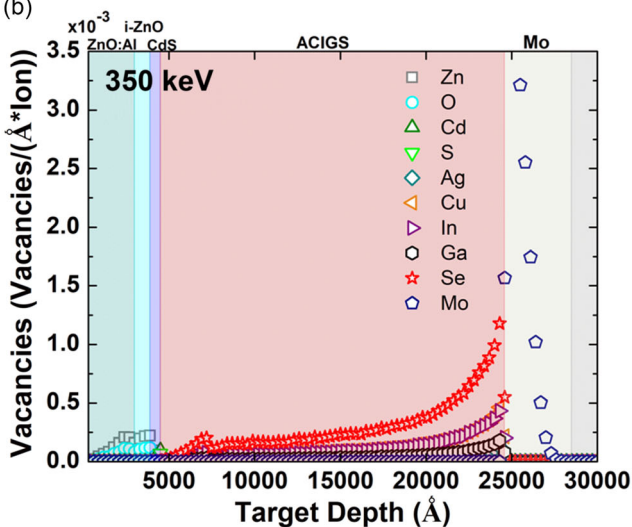


**Figure 2.** Vacancies created by proton interactions during irradiation using SRIM, shown with respect to device structure layers: ZnO:Al/i-ZnO/CdS/ACIGS/Mo for a) 80 keV, which only shows the first three layers and only a small portion of the absorber layer due to the limited damage range of these protons in the structures, and b) upon 350 keV proton irradiation.

temperature, allowing it to move freely until it finds available trapping sites. $^{[18]}$ 

At 80 keV, the majority of protons are expected to become immobilized at the front ZnO/CdS/ACIGS interface. However, previous research suggests that the main defects created in the ZnO due to proton bombardment might exhibit mobility at room temperature in the vicinity of the irradiated area. Consequently, these defects could potentially self-heal or anneal over time. [19]

Likewise, in the case of CdS the bond between Cd and H is not very strong, and there is a chance that a limited fraction of CdH—that is easy to remove—may have bonded and/or get liberated either through additional bombardment, or as a result of

interaction with lattice phonons. [20] As such, only a qualitative description of the phenomenological effects is provided here. Previously, it has been shown that Cd diffuses into the absorber during annealing. [21,22] In these works, a decrease in fill factor (FF) and  $V_{\rm oc}$  was reported in devices where Cd had diffused into the junction through annealing. Importantly, Koprek et al. [21] also highlighted the role of copper vacancies via Cd diffusion into the absorber indicating that the vacancies or defects of greatest interest, are Cd and O vacancies near the top of the cell.

Furthermore, it has been observed that FF losses are explicitly driven by changes to the charge concentration near the interface. [23,24] Specifically, they point to improved performance when soaking the devices under white light due to the removal of the p region at the front of the (A)CIGS layer. Figure 2 shows that in the 80 keV sample there is creation of Cd vacancies and Cu vacancies possibly exaggerating this effect.

Another consideration is the mobility of vacancies created in the ACIGS absorber. Earlier research found the importance of the Ga grading in ACIGS. [25,26] In refs. [25,26], the concentration of Ga defects was shown to affect the bandgap and carrier lifetime of ACIGS significantly. In general, higher concentrations of Ga to In/Ga ratio are associated with shorter carrier lifetimes and a larger bandgap. Typically, CIGS cells are graded front to back with a rich–poor–richer Ga to Ga/In ratio. [8,27,28] This is done to encourage minority carriers, in this case, electrons, in the ACIGS to move toward the CdS/ACIGS interface. [29]

Here, we suggest that low-energy proton radiation inflicts more damage since it deposits all its energy into the device as they are implanted in the absorber region of the device. This damage results in significantly higher nuclear displacement and a high number of nonradiative centers. High-energy protons, while creating ionization damage, are not implanted, and in general, will create fewer vacancies at equivalent fluences. This point is further illustrated by noting that the ACIGS cells studied here were irradiated with lower energy protons than in the earlier studies by Afshari et al.<sup>[9]</sup> and Brown et al.<sup>[3]</sup> However, the behavior of CIGS system independent of irradiation is complex and the operation of these devices is known to be affected by metastability that changes the nature of the p-n junction and background doping profile in the CIGS absorber under illumination or at elevated temperature. [15] As such, the effect of defect generation, metastability, and illumination, under solar irradiation likely generates a complex combination of effects. Here, we evaluate the effects of targeted proton irradiation on the ACIGS devices under investigation, such that role of IEL and NIEL on the structure might be assessed in a more quantitative manner.

Figure 3 shows the current density–voltage (AM 0) responses for two ACIGS solar cells recorded before and after proton irradiation at 80 and 350 keV at 77, 200, and 300 K, respectively. In these Figures, black and green represent the solar cells irradiated with 80 and 350 keV, respectively, while the full and dotted lines indicate before (pre) and after (post) proton radiation. At 77 K, both solar cells display the well-known inflection in the FF, both in the pristine (pre)exposure samples and upon irradiation at both energies. This is attributed to the parasitic nature of the upper CdS/ACIGS interface at lower temperature. Upon exposure, both solar cells measured at 77 K (Figure 3a,b) lose performance suggesting increased nonradiative losses that are

2367198x, 0, Downloaded from https://onlinelibrary.wiley.com/doi/10.1002/solr.202300756 by National Yang Ming Chiao Tung Unive, Wiley Online Library on [18/12/2023]. See the Term

s) on Wiley Online Library for rules of use; OA articles are governed by the applicable Creative Commons

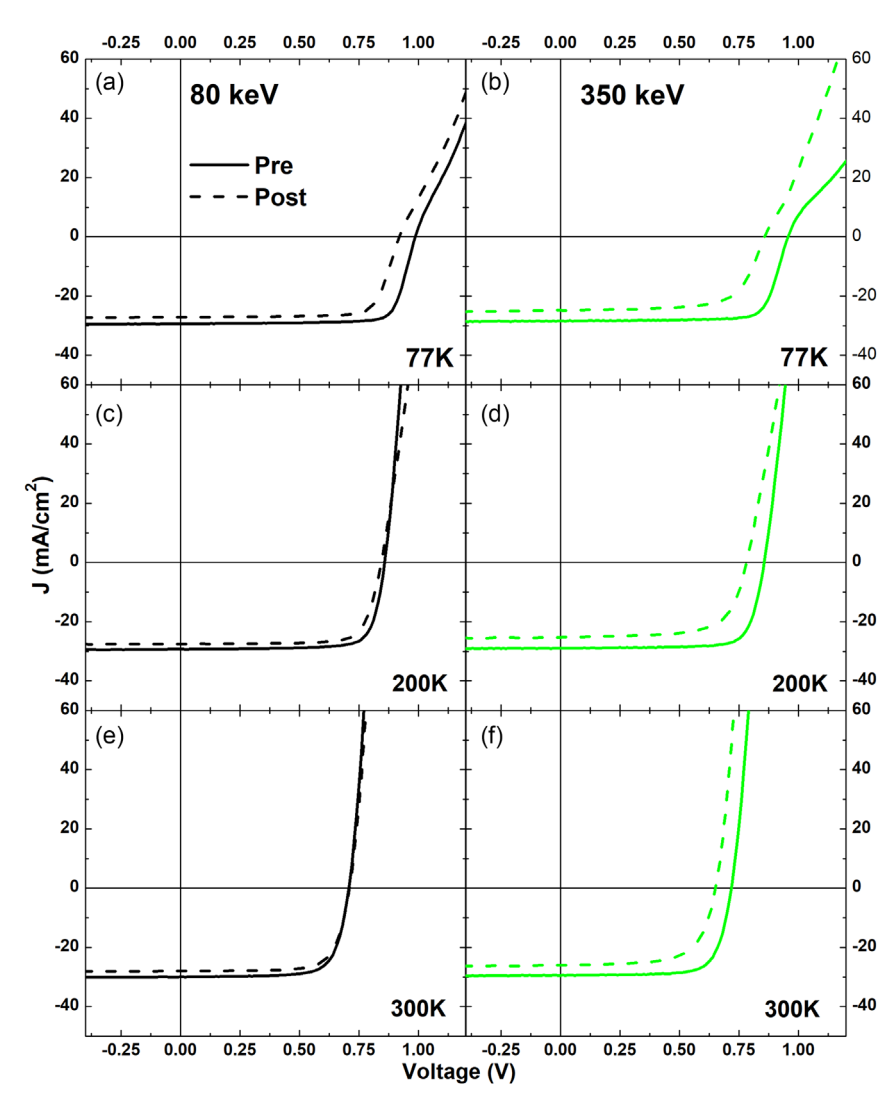


Figure 3. a) Current density versus voltage at selected temperatures of the sample exposed to the 80 keV protons (black) in the left column and the sample that was exposed to 350 keV protons (green) in the right column. The solid lines represent the J-V before irradiation (pre) and the dashed lines after radiation exposure (post). At room temperature (e, f), there is minimal damage. At lower temperatures (a-d), the irradiated sample shows an increase in series resistance and a loss in  $V_{oc}$ .

exacerbated by the low thermal energy, at least in the case of the device irradiated by 80 keV protons. This is supported by improved performance for the solar cells irradiated with 80 keV protons at T > 200 K, as observed in Figure 3c,e. Indeed, at both: (c) 200 K and (e) 300 K, the difference in J-V between pre- and postirradiated is negligible.

However, in the case of the device shown in Figure 3b,d,f, irradiated at higher energy (350 keV), the performance of the device is less than the pristine case (bold versus dashed). Interestingly, the relative performance for this device does not change significantly from 77 to 300 K indicating the loss of  $J_{sc}$  and  $V_{oc}$  (with fixed FF) upon irradiation may have changed the nature of the structure, rather than introduced prohibitive defects into the system—this is discussed in the following paragraphs.

The difference in performance for the two devices exposed to 80 and 350 keV provides insight into the role and nature of radiation-induced defect (vacancy) generation in these devices; and the effect such perturbations have on the transport and interface quality, and/or the ACIGS composition or grading. All these properties are critical for high photovoltaic (PV) performance in CIGS systems. [25,26] In the case of the solar cell exposed to 80 keV protons, the energy loss and defect generation are dominated by NIEL at the upper CdS/CIGS interface and IEL in the ZnO transport layer. The back of the device is relatively unaffected by such exposure. NIEL processes are typically considered the most damaging loss mechanisms in conventional solar cells when exposed to high radiation space conditions, causing nuclear displacement, and increased nonradiative recombination.<sup>[30]</sup> As such, it is somewhat surprising that the ACIGS device exposed to lower energy radiation (80 keV) is observed to retain performance at higher temperatures (200 and 300 K).

Sulai

2367198x, Downloaded from https://oninelibrary.wikey.com/doi/10.1002/sol;202309756 by National Yang Ming Chioa Tung Unive, Wiley Online Library on [18/12/2023]. See the Terms and Conditions (https://onlinelibrary.wikey.com/doi/10.1002/sol;202309756 by National Yang Ming Chioa Tung Unive, Wiley Online Library on [18/12/2023]. See the Terms and Conditions (https://onlinelibrary.wikey.com/doi/10.1002/sol;202309756 by National Yang Ming Chioa Tung Unive, Wiley Online Library on [18/12/2023]. See the Terms and Conditions (https://onlinelibrary.wikey.com/doi/10.1002/sol;202309756 by National Yang Ming Chioa Tung Unive, Wiley Online Library on [18/12/2023]. See the Terms and Conditions (https://onlinelibrary.wikey.com/doi/10.1002/sol;202309756 by National Yang Ming Chioa Tung Unive, Wiley Online Library on [18/12/2023]. See the Terms and Conditions (https://onlinelibrary.wikey.com/doi/10.1002/sol;202309756 by National Yang Ming Chioa Tung Unive, Wiley Online Library on [18/12/2023]. See the Terms and Conditions (https://onlinelibrary.wikey.com/doi/10.1002/sol;202309756 by National Yang Ming Chioa Tung Unive, Wiley Online Library on [18/12/2023]. See the Terms and Conditions (https://onlinelibrary.wikey.com/doi/10.1002/sol;202309756 by National Yang Ming Chioa Tung Unive, Wiley Online Library on [18/12/2023]. See the Terms and Conditions (https://onlinelibrary.wikey.com/doi/10.1002/sol;202309756 by National Yang Ming Chioa Tung Unive, Wiley Online Library on [18/12/2023]. See the Terms and Conditions (https://onlinelibrary.wikey.com/doi/10.1002/sol;20230976 by National Yang Ming Chioa Tung Unive, Wiley Online Library on [18/12/2023]. See the Terms and Conditions (https://onlinelibrary.wikey.com/doi/10.1002/sol;20230976 by National Yang Ming Chioa Tung Unive, Wiley Online Library on [18/12/2023]. See the Terms and Conditions (https://onlinelibrary.wikey.com/doi/10.1002/sol;20230976 by National Yang Ming Chioa Tung University (https://onlinelibrary.wikey.com/doi/10.1002/sol;20230976 by National Yang Ming Chioa Tung Unive

www.advancedsciencenews.com www.solar-rrl.com

To understand this behavior, the nature of (A)CIGS, its metastability, and the low formation energy of defects in these systems need to be considered. The SRIM analysis provided in Figure 2 indicates that upon proton irradiation, Cu vacancies are among the most plentiful generated in the ACIGS absorber. Cu defects are known to have a low formation energy in these systems, are highly mobile, and are known to have a significant effect on the p-type nature of these materials. Specifically, Cu-vacancies have been suggested to create a "p+" region close to the CdS/absorber junction that results in a thin interfacial region of (A)CIGS that is more p-type than the rest of the bulk.[31,32] The formation of a highly dense acceptor region close to the interface can facilitate electron tunneling through the CdS/CIGS interface, while Cu vacancies were also likely to redistribute in the p region affecting the nature and position of the p-n junction, and depletion region something previously invoked to explain the improve performance of CIGS after red light soaking.[15]

IEL processes in and around the ZnO transporting layer and interface may also improve the system via local heating, something also observed to improve interfaces in (and at) TCO transporting layers and interfaces in metal halide perovskite interfaces. [13,33,34] A combination of local annealing and improved transport across the upper CdS/ACIGS layer mediated by the irradiation of the device with 80 keV is consistent with the data presented. At 77 K (see Figure 3a), a reduction in the J-V response is observed. Here, we postulate that this is likely due to the radiation-induced defect generation and the role this has in perturbing the doping profile at and around the CdS/ ACIGS interface, which either pins or lowers the Fermi-level such that there is a lower effective bandgap and therefore reduced  $J_{\rm sc}$  and  $V_{\rm oc}$  with respect to the preirradiated sample. At higher temperatures (T = 200 and 300 K), the Fermi-level increases and this coupled with the thermal energy of carriers reduces the parasitic losses observed at lower temperature. Indeed, at T = 200 and 300 K, shown in Figure 3c,e, respectively, the sample irradiated at 80 keV shows little change in before and after radiation exposure, indicating reasonable radiation tolerance at lower energy. The hypothesis that exposure to 80 keV protons facilitates transport and carrier extraction at the CdS/CIGS interface is further supported by EQE measurements for solar cells exposed to 80 keV protons measured at 77, 100, and 200 K, which are shown in Figure 4a,c,e, respectively.

In all cases, there is a clear improvement in the EQE response after exposure to 80 keV irradiation (black dashed lines). Since this occurs across all wavelengths, it indicates the presence and removal of a parasitic barrier to minority carrier extraction after radiation exposure, which supports the improvement in carrier extraction at the CdS/ACIGS barrier described with respect to the EQE measurements above. However, it is possible to raise an argument regarding the decline in  $J_{\rm sc}$  when comparing the pre- and post-80 keV exposure states of the device, as depicted in Figure 3a,c,e, despite a notable enhancement in EQE, as shown in Figure 4a,c,e.

This disparity could arise from various potential factors, and the ultimate behavior of the devices may result from the combined effects of these factors. The first factor to consider is the damage incurred at the contacts. In the case of the 80 keV

exposure, the majority of the damage is concentrated at the front of the device, with a significant amount of damage occurring in the top contact layer (while the back contact remains unaffected). This concentrated damage may have negatively impacted the quality of the ohmic contact compared to the 350 keV exposure, where the entire device experiences damage, likely resulting in more extensive damage to both contacts as well as throughout the bulk of the device.

Another plausible factor contributing to this effect could be the inability to efficiently extract all charge carriers, particularly when the charge transport is hindered by increased carrier generation. The current flowing through the solar cell is constrained by the transport processes across the buffer layer and its interfaces. The density of charge carriers available for transport within the buffer layer can be influenced by the extent of damage within the bulk of the buffer layer, potentially leading to a depletion of charge carriers in the buffer when higher charge generation rates are encountered. [35] When considering the identical ACIGS solar cell exposed to 350 keV, there are clear differences with that of the lower energy (80 keV) exposed solar cell. As shown in Figure 3b, the sample exposed to 350 keV shows a typical lowtemperature inflection due to the parasitic effects of the upper heterointerface at 77 K the resistance of which, despite the loss of PV response, is reduced upon irradiation (green dashes). At 200 and 300 K, shown in Figure 3d,f, respectively, both  $I_{sc}$  and  $V_{\rm oc}$  are reduced after radiation exposure, but the FF is apparently relatively unaffected at all temperatures after 350 keV exposure.

When comparing the EQE (green) of the ACIGS solar cell exposed to higher proton energy (350 keV) at 77, 200, and 300 K in Figure 4b,d,f, respectively to their associated *I*–*V* in Figure 3, the differences with respect to the solar cell exposed to 80 keV protons are evident. Consistent with their J-V, the EQE for the pristine (pre-IRR) solar cells (solid green) are affected in a similar way at all temperatures after exposure to radiation (green dashes). Specifically, while low-energy irradiation showed little loss, indeed improvement in the EQE upon exposure (black dashes - Figure 4a,c,e) the EQE exposed to 350 keV is improved after (post-IRR) irradiation (green dashes) at the wavelengths below  $\approx$ 500 nm and reduced at wavelengths longer than ≈800 nm, indicative of a larger number of vacancies in the quasi-neutral region of the absorber. Between these regimes (500-800 nm), the EQE is relatively unaffected by radiation exposure at 350 keV for the fluence provided.

To understand the effect of radiation at 350 keV on the device, the SRIM calculations in Figure 1 and 2 should be considered. In Figure 1d, the contribution of IEL and NIEL are shown across the device structure for the higher radiation exposure. Contrary to the case of the solar cell exposed to 80 keV, in the case of 350 keV exposure, the protons travel deep into the cell structure and terminate in the Mo back transport layer (see trajectory in Figure 1b), and significant energy is dissipated via NIEL processes (open red stars) at the back of the ACIGS absorber. Although it is hypothesized that the annealing effects of the IEL at the ACIGS/Mo interface might work similarly to what was observed with the 80 keV exposure at the CdS/ACIGS interface, potentially leading to improvements in the back interface of the device, this effect becomes more apparent when Figure 3a,b are compared.

2367198x, 0, Downloaded from https://onlinelibrary.wiley.com/doi/10.1002/solr.202300756 by National Yang Ming Chiao Tung Unive, Wiley Online Library on [18/12/2023]. See the Term

ns) on Wiley Online Library for rules of use; OA articles are governed by the applicable Creative Commons I

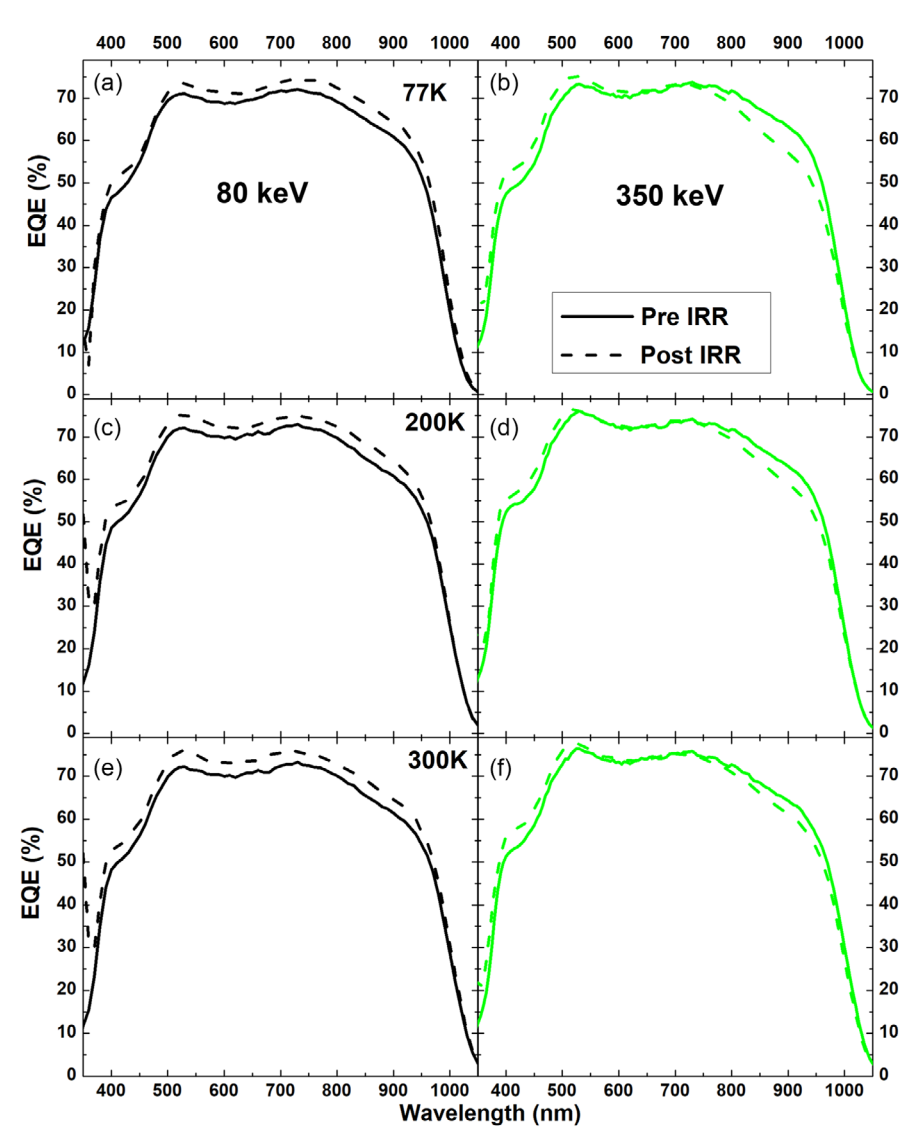


Figure 4. EOE at selected temperatures for the sample exposed to 80 keV protons (black, a, c, e) in the left column and samples exposed to 350 keV protons (green, b, d, f) in the right column. The solid lines show the EQE before (pre-IRR) irradiation, and the dashed lines after irradiation (post-IRR). In the sample exposed to the 80 keV protons, there is an improvement seen across the whole EQE. While in the sample exposed to the 350 keV protons, there is some improvement in the 400-525 nm range, and a reduction in extraction of electrons excited by wavelengths longer than 800 nm.

Notably, there is a significant enhancement in the I-V kink observed with the 350 keV exposure. This kink in the *I*–*V* curve, which has previously been linked to the barrier for hole extraction at the Mo back contact, may have been somewhat improved by the IEL processes. [36] However, the interplay between the extent of IEL and NIEL effects is complex and likely depends on the type of interface. It is also worth noting that the NIEL damage remains consistent throughout the device during the 350 keV exposure, possibly outweighing the healing effects of IEL in this particular device. In addition, since the protons travel through the full stack, the structure also experiences considerable IEL (open black squares) at the upper CdS/ACIGS interface and into the bulk of the ACIGS absorber.

In Figure 1c,d, the absorption depth of blue (dotted line) and red (dashed) light are shown as calculated using transfer matrix simulations. These calculations show that excitation (or losses at solar energy) wavelengths in the visible are affected predominately by IEL in the solar cell exposed to 350 keV. As such, the EQE measured in this region also enables the effects of IEL on the device to be decoupled and evaluated, while at >800 nm NIEL processes are probed. IEL processes, in addition to creating vacancies, generate considerable heat that appears to facilitate improvements in the interface properties and reduce nonradiative losses in the p-region and at the CdS/ACIGS heterointerface, in the samples under investigation here. This is reflected in the softening of the J-V kink upon irradiation, as shown in Figure 3b. As such, here, it is postulated that this serves-in a similar vein to the effects observed under 80 keV irradiation in Figure 4e, for example—to improve the carrier extraction and transport at the upper CdS/ACIGS

2367198x, 0, Downloaded from https://onlinelibrary.wiley.com/doi/10.1002/solt-202300736 by National Yang Ming Chiao Tung Unive, Wiley Online Library on [18/12/2023]. See the Terms and Conditions (https://onlinelibrary.wiley.com/erms

-and-conditions) on Wiley Online Library for rules of use; OA articles are governed by the applicable Creative Commons License

interface and reduces losses in the upper region of ACIGS absorber.

In terms of the absorber, while the formation energy of defects is low in ACIGS, and inevitably increased by IEL, these complexes and the inherent metastability of this material also likely facilitate the annealing of nonradiative centers and reconstruction or passivation of defects, at least at the fluence used here. However, the performance if the device is ultimately limited by NIEL processes that prove prohibitive at the rear of the solar cell. These hypotheses are supported at least partially by the evident increase in EQE response in the blue region of the EQE (<500 nm) after irradiation (dashed lines), and the apparent lack of any loss of collection between 500 and 800 nm, as shown under irradiation in Figure 4b,d,f; wavelengths that represent the upper (p-region) and mid-point (intrinsic) regions of the structure.

When considering the longer wavelength regime of the EQE upon high(er) energy irradiation, loss of EQE and therefore carrier collection is evident. This likely occurs due to NIEL that affects the rear of the solar cell as indicated by the SRIM in Figure 1d. The net result appears to be a combination of loss of transport in the back, hole extraction layers, and/or defect formation in ACIGS layer at the ACIGS/Mo interface, in the base of the cell. The SRIM calculations in Figure 2b show several elemental vacancies generated by NIEL in the ACIGS base region including considerable In and Se vacancies, in addition to Cu and Se, suggesting significant decomposition or modulation of the ACIGS absorber at the back of the solar cell. Since the grading of the ACIGS is a standard design protocol in CIGS-based solar cells,  $^{[37-39]}$  and the Ga to Ga/In ratio is carefully controlled in these systems to facilitate minority carrier extraction, defect generation, and the modification of the In and Ga profile in the base region of the device likely affect carrier extraction, which is known to negatively affect device performance.<sup>[40]</sup>

While the exact nature of the redistribution of the group III elements relative to one another, in addition to Cu and/or Se requires further materials analysis upon radiation, the EQE supports the suggested decomposition of the ACIGS at the rear and throughout the absorber of the solar cell and perturbations at the ACIGS/Mo interface at prohibitively affected by NIEL under irradiation. The *J*–V measurements shown in Figure 3 for the solar cell irradiated at 350 keV indicate any positive effects of IEL-driven annealing at the top emitter region of the structure, are dominated by losses due to NIEL in the lower base region of the device. Some difference in the *J*–*V* and EQE can be accounted for by the effects of low-power monochromatic excitation under monochromatic excitation used in the EQE measurement versus the broadband illumination at AM0 excitation from the solar simulator used to record *I*–*V* measurements.

However, the difference in carrier extraction under monochromatic versus broadband illumination (particularly after 80 keV irradiation) likely reflects the competition between carrier generation and thermionic emission at the interface, in which larger carrier generation induces high parasitic resistances as carriers build up and the heterointerface due to low thermionic emission rates. Such behavior has also recently been observed in perovskites at low temperatures. [41,42] This behavior is qualitatively supported by both the data and SRIM calculations which indicate that the upper emitter layer of the structure is more robust to both NIEL and IEL damage than the lower base presumably because of deleterious NIEL on the ACIGS compositional profile.

#### 4. Conclusion

Here, commercial-grade ACIGS solar cells are assessed using targeted proton irradiation on the interfaces of the ACIGS and emitter and base regions to evaluate the stability and impact upon these regions in the structure to investigate the stability of such systems for space applications. Interestingly, irradiation with 80 keV particles that stop close to the CdS/ACIGS interfaces provides little effect upon performance at the fluence levels used. This unexpected behavior is attributed to local annealing of the ZnO/CdS/ACIGS interface combined with local changes in the doping profile under irradiation that appear to facilitate carrier extraction across the heterointerface in the upper emitter region of the structure.

However, the irradiation at higher energy (350 keV) used here while affecting the full absorber layer will be particularly parasitic and target the base region of the structure reducing the performance of the solar cells and observed in the *J*–V measurements after proton exposure. While the EQE measurements indicated heating due to IEL in the upper emitter region of the devices improved collection in this region of the device, significant loss of extraction was evident deeper in the structure due to NIEL, which is attributed to radiation-induced defects and their role in changing the Ga to In/Ga ratio in the base region of the absorber and at the ACIGS/Mo interface.

## Acknowledgements

The authors thank the funding support of the National Aeronautics and Space Administration under Agreement No. 80NSSC19M0140 issued through NASA Oklahoma EPSCoR, Support is also acknowledged through SEED funding from the Center for Quantum Research and Technology (CQRT) at the University of Oklahoma. UNT acknowledges partial support from NSF grant No. ECCS-2210722.

#### Conflict of Interest

The authors declare no conflict of interest.

### **Data Availability Statement**

The data that support the findings of this study are available from the corresponding author upon reasonable request.

# **Keywords**

ACIGS, interfaces, radiation, stability, temperatures

Received: September 22, 2023 Revised: November 13, 2023 Published online:



Solar

2367 198x, 0, Downloaded from https://onlinelibrary.wiley.com/doi/10.1002/solr.202300756 by National Yang Ming Chiao Tung Unive, Wiley Online Library on [18/12/2023]. See the Terms and Conditions (https://onlinelibrary.wiley.com/doi/10.1002/solr.202300756 by National Yang Ming Chiao Tung Unive, Wiley Online Library on [18/12/2023]. See the Terms and Conditions (https://onlinelibrary.wiley.com/doi/10.1002/solr.202300756 by National Yang Ming Chiao Tung Unive, Wiley Online Library on [18/12/2023]. See the Terms and Conditions (https://onlinelibrary.wiley.com/doi/10.1002/solr.202300756 by National Yang Ming Chiao Tung Unive, Wiley Online Library on [18/12/2023].

governed by the applicable Creative Commons

www.advancedsciencenews.com www.solar-rrl.com

- [1] NREL, Best Research-Cell Efficiency Chart, US Department of Energy, https://www.nrel.gov/pv/cell-efficiency.html (accessed: December 2023).
- [2] H. Shen, T. Duong, J. Peng, D. Jacobs, N. Wu, J. Gong, Y. Wu, S. K. Karuturi, X. Fu, K. Weber, X. Xiao, T. P. White, K. Catchpole, Energy Environ. Sci. 2018, 11, 394.
- [3] C. R. Brown, V. R. Whiteside, D. Poplavskyy, K. Hossain, M. S. Dhoubhadel, I. R. Sellers, IEEE I. Photovoltaics 2019, 9, 552.
- [4] C. P. Thompson, L. Chen, W. N. Shafarman, J. Lee, S. Fields, R. W. Birkmire, in 2015 IEEE 42nd Photovoltaic Specialist Conf. (PVSC), IEEE, Piscataway, NI 2015.
- [5] M. Edoff, T. Jarmar, N. S. Nilsson, E. Wallin, D. Hogstrom, O. Stolt,
  O. Lundberg, W. Shafarman, L. Stolt, *IEEE J. Photovoltaics* 2017, 7,
- [6] P. T. Erslev, J. Lee, G. M. Hanket, W. N. Shafarman, J. D. Cohen, *Thin Solid Films* 2011, 519, 7296.
- [7] N. Valdes, J. Lee, W. Shafarman, Sol. Energy Mater. Sol. Cells 2019, 195, 155.
- [8] Y. Zhao, S. Yuan, D. Kou, Z. Zhou, X. Wang, H. Xiao, Y. Deng, C. Cui, Q. Chang, S. Wu, ACS Appl. Mater. Interfaces 2020, 12, 12717.
- [9] H. Afshari, B. K. Durant, C. R. Brown, K. Hossain, D. Poplavskyy, B. Rout, I. R. Sellers, Sol. Energy Mater. Sol. Cells 2020, 212, 110571.
- [10] J. M. Young, T. A. Byers, E. J. Lang, S. Singh, G. A. Glass, K. Hattar, B. Rout, *Planet. Space Sci.* **2021**, 206, 105319.
- [11] J. F. Ziegler, M. D. Ziegler, J. P. Biersack, Nucl. Instrum. Methods Phys. Res., Sect. B 2010, 268, 1818.
- [12] S.-I. Sato, K. Beernink, T. Ohshima, in 2013 IEEE 39th Photovoltaic Specialists Conf. (PVSC) PART 2, IEEE, Piscataway, NJ 2013.
- [13] B. K. Durant, H. Afshari, S. Singh, B. Rout, G. E. Eperon, I. R. Sellers, ACS Energy Lett. 2021, 6, 2362.
- [14] S.-I. Sato, K. Beernink, T. Ohshima, Jpn. J. Appl. Phys. 2015, 54, 061401.
- [15] S. Lany, A. Zunger, J. Appl. Phys. 2006, 100, 113725.
- [16] J. Pohl, K. Albe, Phys. Rev. B 2013, 87, 245203.
- [17] A. K. Singh, A. Janotti, M. Scheffler, C. G. Van De Walle, Phys. Rev. Lett. 2008, 101, 055502.
- [18] J. Bo/Ttiger, S. T. Picraux, N. Rud, T. Laursen, J. Appl. Phys. 1977, 48, 920.
- [19] F. D. Auret, S. A. Goodman, M. Hayes, M. J. Legodi, H. A. Van Laarhoven, D. C. Look, Appl. Phys. Lett. 2001, 79, 3074.
- [20] J. Tatarkiewicz, A. Breitschwerdt, A. Witowski, Phys. Rev. B 1989, 39, 3889.
- [21] A. Koprek, O. Cojocaru-Miredin, R. Wuerz, C. Freysoldt, B. Gault, D. Raabe, *IEEE J. Photovoltaics* 2017, 7, 313.

- [22] K. Lee, E.-A. Ok, J.-K. Park, W. M. Kim, Y.-J. Baik, D. Kim, J.-H. Jeong, Appl. Phys. Lett. 2014, 105, 083906.
- [23] M. Igalson, M. Bodegård, L. Stolt, Sol. Energy Mater. Sol. Cells 2003, 80, 195.
- [24] P. Jackson, R. Wuerz, D. Hariskos, E. Lotter, W. Witte, M. Powalla, Phys. Status Solidi RRL 2016, 10, 583.
- [25] L. Kronik, U. Rau, J.-F. Guillemoles, D. Braunger, H.-W. Schock, D. Cahen, Thin Solid Films 2000, 361, 353.
- [26] Y.-H. Chang, R. Carron, M. Ochoa, C. Bozal-Ginesta, A. N. Tiwari, J. R. Durrant, L. Steier, Adv. Energy Mater. 2021, 11, 2003446.
- [27] A. Chirilă, S. Buecheler, F. Pianezzi, P. Bloesch, C. Gretener, A. R. Uhl, C. Fella, L. Kranz, J. Perrenoud, S. Seyrling, R. Verma, S. Nishiwaki, Y. E. Romanyuk, G. Bilger, A. N. Tiwari, *Nat. Mater.* 2011, 10, 857.
- [28] M. Murata, D. Hironiwa, N. Ashida, J. Chantana, K. Aoyagi, N. Kataoka, T. Minemoto, Jpn. J. Appl. Phys. 2014, 53, 04ER14.
- [29] J. Song, S. S. Li, C. H. Huang, O. D. Crisalle, T. J. Anderson, Solid-State Electron. 2004, 48, 73.
- [30] S. R. Messenger, G. P. Summers, E. A. Burke, R. J. Walters, M. A. Xapsos, Prog. Photovoltaics 2001, 9, 103.
- [31] S. Ishizuka, P. J. Fons, Phys. Rev. Appl. 2021, 15, 054005.
- [32] A. O. Pudov, A. Kanevce, H. A. Al-Thani, J. R. Sites, F. S. Hasoon, J. Appl. Phys. 2005, 97, 064901.
- [33] B. K. Durant, H. Afshari, S. Sourabh, V. Yeddu, M. T. Bamidele, S. Singh, B. Rout, G. E. Eperon, D. Y. Kim, I. R. Sellers, Sol. Energy Mater. Sol. Cells 2021, 230, 111232.
- [34] V. V. Brus, F. Lang, J. Bundesmann, S. Seidel, A. Denker, B. Rech, G. Landi, H. C. Neitzert, J. Rappich, N. H. Nickel, Adv. Electron. Mater. 2017, 3, 1600438.
- [35] A. Villanueva-Tovar, T. Kodalle, C. A. Kaufmann, R. Schlatmann, R. Klenk, Sol. RRL 2020, 4, 1900560.
- [36] T. Schneider, C. Dethloff, T. Hölscher, H. Kempa, R. Scheer, Prog. Photovoltaics 2022, 30, 191.
- [37] O. Lundberg, M. Edoff, L. Stolt, Thin Solid Films 2005, 480, 520.
- [38] T. Feurer, P. Reinhard, E. Avancini, B. Bissig, J. Löckinger, P. Fuchs, R. Carron, T. P. Weiss, J. Perrenoud, S. Stutterheim, S. Buecheler, A. N. Tiwari, *Prog. Photovoltaics* 2017, 25, 645.
- [39] N. E. Gorji, M. D. Perez, U. Reggiani, L. Sandrolini, Int. J. Eng. Technol. 2012, 4, 573.
- [40] M. Gloeckler, J. R. Sites, J. Phys. Chem. Solids 2005, 66, 1891.
- [41] H. Afshari, B. K. Durant, A. R. Kirmani, S. A. Chacon, J. Mahoney, V. R. Whiteside, R. A. Scheidt, M. C. Beard, J. M. Luther, I. R. Sellers, ACS Appl. Mater. Interfaces 2022, 14, 44358.
- [42] C. R. Brown, G. E. Eperon, V. R. Whiteside, I. R. Sellers, ACS Appl. Energy Mater. 2019, 2, 814.